J. Math. Biol.
DOI 10.1007/s00285-011-0401-0

Mathematical Biology

The surface finite element method for pattern formation on evolving biological surfaces

R. Barreira · C. M. Elliott · A. Madzvamuse

Received: 5 May 2010 / Revised: 4 December 2010

Abstract In this article we propose models and a numerical method for pattern formation on evolving curved surfaces. We formulate reaction-diffusion equations on evolving surfaces using the material transport formula, surface gradients and diffusive conservation laws. The evolution of the surface is defined by a material surface velocity. The numerical method is based on the evolving surface finite element method. The key idea is based on the approximation of Γ by a triangulated surface Γ_h consisting of a union of triangles with vertices on Γ. A finite element space of functions is then defined by taking the continuous functions on Γ_h which are linear affine on each simplex of the polygonal surface. To demonstrate the capability, flexibility, versatility and generality of our methodology we present results for uniform isotropic growth as well as anisotropic growth of the evolution surfaces and growth coupled to the solution of the reaction-diffusion system. The surface finite element method provides a robust numerical method for solving partial differential systems on continuously evolving domains and surfaces with numerous applications in developmental biology, tumour growth and cell movement and deformation.

R. Barreira
Escola Superior de Tecnologia do Barreiro/IPS, Rua Américo da Silva Marinho-Lavradio, 2839-001 Barreiro, Portugal
e-mail: raquel.barreira@estbarreiro.ips.pt

C. M. Elliott
Mathematics Institute and Centre for Scientific Computing, University of Warwick, Coventry CV4 7AL, UK
e-mail: C.M.Elliott@warwick.ac.uk

A. Madzvamuse (✉)
Department of Mathematics, University of Sussex, Falmer, Brighton, BN1 9QH, UK
e-mail: a.madzvamuse@sussex.ac.uk

Published online: 28 January 2011

Keywords Pattern formation · Evolving surfaces · Surface finite element method · Reaction-diffusion systems · Activator-depleted model

Mathematics Subject Classification (2000) 35K57 · 35K58 · 37C60 · 65M60 · 9108 · 9208

1 Introduction

The purpose of this paper is to formulate reaction-diffusion equations on evolving surfaces and to propose a novel numerical approach based on the *surface finite element method*. The context is that of pattern formation on a growing biological surface modelled by reaction-diffusion equations following the classical paper of Turing (1952). Such equations exhibit diffusion-driven instability of spatially uniform structures leading to spatially non-uniform patterns. Many mathematical models based upon this work were later developed and analysed motivated by applications such as pattern formation in hydra, sequential pattern formation in vertebrates, coat markings of animals and pigmentation patterns on butterfly wings, amongst others. For an overview we refer the reader to Murray (2002).

The original work of Turing did not take into account growth and changes in geometry. However, these factors are important in the development of patterns observed in nature. Pattern formation on growing domains has been widely studied. For example Crampin et al. (1999) considers domain growth for a one-dimensional domain and shows that it may be a mechanism for increasing the robustness of pattern formation with respect to the initial conditions. In the context of understanding the evolution of the stripes observed in the fish Pomacanthus (Kondo and Asai 1995), a two-dimensional growing planar domain was considered in Maini et al. (1997). See also Madzvamuse et al. (2009) where the Turing diffusively-driven instability conditions are generalised to reaction-diffusion systems with slow, isotropic domain growth. The numerical method proposed in this article is a tool to explore such reaction kinetics on evolving surfaces.

Much interesting work has been carried out for growing planar domains. However in applications to biological forms it is natural to consider pattern formation on an evolving curved surface which is the boundary of a growing three-dimensional domain. For example we refer to Aragón et al. (1999) and Barrio et al. (2004) where the effects of curvature in the selection of patterns on a stationary sphere and growing cones were studied. Another initial study is the work in Chaplain et al. (2001) which presents a numerical method for the problem of pattern formation on spherical surfaces with applications to solid tumour growth. Their numerical method is based on parameterising the surface over a sphere and then using the method of lines.

Our approach is based on the surface finite element method which is a natural extension of the finite element method (Madzvamuse et al. 2003) and is capable of handling complex geometries and shapes (Dziuk and Elliott 2007a,b; Eilks and Elliott 2008; Barrett et al. 2008; Barreira 2009; Elliott and Stinner 2010). The idea is to triangulate the surface and approximate the system of partial differential equations using piece-wise linear surface finite element spaces based on the triangulation. In this paper we are interested in evolving surfaces. In this instance the vertices of the triangulation

are moved with a velocity which is either prescribed or is governed by some evolution law. In order to do this we need to formulate an appropriate conservation law on the surface. The evolving surface finite element method exploits the special features of this conservation law when written in an appropriate variational form.

The reaction-diffusion equations on evolving surfaces are formulated in Sect. 2. Within this framework we establish appropriate notation for surface gradients which is key to deriving from first principles reaction-diffusion systems on evolving surfaces. For illustrative purposes we consider the well-studied *activator-depleted* substrate model (Gierer and Meinhardt 1972; Prigogine et al. 1968; Schnakenberg 1979) also known as the Brusselator model as a reaction-kinetic candidate for exploration. Similarly, any other plausible reaction kinetics can be easily treated in this framework. We also discuss the formulation of models for surface growth.

In Sect. 3 we present the *evolving surface finite element method* applied to reaction-diffusion systems on evolving surfaces which change shape. A feature of the variational formulation is that certain geometric quantities such as the mean curvature and normal of the surface do not appear. This is then taken advantage of in a natural way by the finite element method. In this approach no transformations or parameterisations are required in formulating either the reaction-diffusion system or the surface finite element method. Discretising in space results in a system of nonautonomous ordinary differential equations which is discretised in time. In particular because this application involves semilinear parabolic equations we linearise nonlinear kinetics following Madzvamuse (2006) to obtain a linear algebraic system. This system is then solved using the GMRes algorithm (Golub and Van Loan 1996).

In Sect. 4 we present Turing patterns on fixed and evolving surfaces. We demonstrate the general applicability of the surface finite element method which has the capability of handling anisotropic growth that might result from biological models. Our results confirm that incorporating domain growth enhances the pattern selection process. The methodology is also applicable to models which couple the surface evolution to the reaction-diffusion system on the surface. This is illustrated in Sect. 5 with an application to modelling growth of solid tumours. Some concluding remarks are made in Sect. 6.

Examples of other articles which also consider the numerical solution of surface partial differential equations include (Greer et al. 2006; Calhoun and Helzel 2009; Dziuk and Elliott 2010; Lefevre and Mangin 2010; Elliott et al. 2010). The article (Deckelnick et al. 2005) is a review of differing approaches to the computation of evolving surfaces.

1.1 Software package

The computations described here were carried-out in the framework of the finite element software package ALBERTA (Schmidt and Siebert 2005).

2 Derivation of the reaction-diffusion equations on an evolving surface

Because we are dealing with surface partial differential equations we need the concepts of hypersurfaces and surface gradients. We establish the notation to

be used throughout the paper in the next section following the accounts in Deckelnick et al. (2005),Dziuk and Elliott (2007a,b) and the references therein. A feature of this approach is the avoidance of the use of parameterisations and charts.

2.1 Surface gradients

A subset $\Gamma \subset \mathbb{R}^3$ is called a $\mathcal{C}^2$-hyper-surface if it can be locally represented as the graph of a $\mathcal{C}^2$-function over an open subset of $\mathbb{R}^2$. For convenience we will assume that Γ can be globally represented as the zero level set of a function d, that is, there exists an open set $\mathcal{U} \subset \mathbb{R}^3$ and a function $d \in C^2(\mathcal{U})$ such that

$$\mathcal{U} \cap \Gamma = \{x \in \mathcal{U} : \ d(x) = 0\}, \quad \text{and} \quad \nabla d(x) \neq 0, \quad \forall\, x \in \mathcal{U} \cap \Gamma.$$

The tangent space at $x \in \Gamma$ is the linear subspace of $\mathbb{R}^3$ that is orthogonal to $\nabla d(x)$ (and is independent of the particular choice of d). A $\mathcal{C}^2$-hyper-surface is called *orientable* if there exists a vector field $\boldsymbol{\nu} \in C^1(\mathbb{R}^3)$ such that $\boldsymbol{\nu}(x)$ is orthogonal to the tangent space and $|\boldsymbol{\nu}(x)| = 1$ for all $x \in \Gamma$. The orientation of Γ is determined by choosing the normal $\boldsymbol{\nu}$ to be in the direction of increasing d and we define the unit normal vector field by

$$\boldsymbol{\nu}(x) = \frac{\nabla d(x)}{|\nabla d(x)|}.$$

One possible choice for d is the signed distance function to Γ and in that case $|\nabla d(x)| = 1$, $\forall\, x \in \Gamma$.

We define the tangential gradient of a function η which is differentiable in an open neighbourhood of Γ by

$$\nabla_\Gamma \eta(x) = \nabla \eta(x) - \nabla \eta(x) \cdot \boldsymbol{\nu}(x) \boldsymbol{\nu}(x), \quad x \in \Gamma,$$

where ∇ denotes the usual gradient in $\mathbb{R}^3$. Note that $\nabla_\Gamma \eta$ has three components and that although the definition relies on extending η off the surface, $\nabla_\Gamma \eta$ depends only on the surface values of η. We will use the following notation

$$\nabla_\Gamma \eta(x) = \left(\underline{D}_1 \eta(x), \underline{D}_2 \eta(x), \underline{D}_3 \eta(x)\right).$$

If η is twice differentiable in an open neighbourhood of Γ, then the *Laplace-Beltrami* operator is defined as the tangential divergence of the tangential gradient:

$$\Delta_\Gamma \eta(x) = \nabla_\Gamma \cdot \nabla_\Gamma \eta(x) = \sum_{i=1}^{3} \underline{D}_i \underline{D}_i \eta(x).$$

2.2 Reaction-diffusion systems on evolving surfaces

Let $\Gamma(t)$ be an evolving two-dimensional hypersurface in $\mathbb{R}^3$ bounding a time-dependent domain $\Omega(t)$ with unit outward pointing normal $\boldsymbol{\nu}$. Let the velocity of

material points on $\Gamma(t)$ be denoted by $\boldsymbol{v} := V\boldsymbol{\nu} + \boldsymbol{v}_T$ where $\boldsymbol{\nu}$ is the unit outward pointing normal to $\Omega(t)$, V is the normal velocity and $\boldsymbol{v}_T$ is a velocity field tangential to the surface and hence orthogonal to $\boldsymbol{\nu}$. We follow the derivation in Dziuk and Elliott (2007a, 2010).

Let $\boldsymbol{u}$ be a vector of scalar concentration fields $\{u_i\}_{i=1}^m$. For each concentration we have a mass conservation law which balances the rate of change of the concentration in an evolving material region with the outward flux and a net reactive production rate $f_i(\boldsymbol{u})$. Let $\mathcal{R}(t)$ be an arbitrary material portion of $\Gamma(t)$ where each point moves with the material velocity. According to the mass balance conservation law,

$$\frac{d}{dt}\int\limits_{\mathcal{R}(t)} u_i = -\int\limits_{\partial\mathcal{R}(t)} \boldsymbol{q}_i\cdot\boldsymbol{\mu} + \int\limits_{\mathcal{R}(t)} f_i(\boldsymbol{u}), \tag{1}$$

where, for each component i, $\boldsymbol{q}_i$ and $f_i(\boldsymbol{u})$ are, respectively, the surface flux through the boundary of $\mathcal{R}(t)$ and the net production rate within the surface. The components of $\boldsymbol{q}$ normal to Γ do not contribute to the flux so we can assume $\boldsymbol{q}$ is a tangent vector. Using integration by parts it follows that

$$\int\limits_{\partial\mathcal{R}(t)} \boldsymbol{q}\cdot\boldsymbol{\nu} = \int\limits_{\mathcal{R}(t)} \nabla_\Gamma\cdot\boldsymbol{q} + \int\limits_{\mathcal{R}(t)} \boldsymbol{q}\cdot\boldsymbol{\nu}H = \int\limits_{\mathcal{R}(t)} \nabla_\Gamma\cdot\boldsymbol{q}.$$

On the other hand, for the left-hand side of (1), we use the transport formula (cf. Dziuk and Elliott 2007b)

$$\frac{d}{dt}\int\limits_{\mathcal{R}(t)} \eta = \int\limits_{\mathcal{R}(t)} \partial^\bullet\eta + \eta\nabla_\Gamma\cdot\boldsymbol{v}$$

for any material region of the surface evolving with the material velocity $\boldsymbol{v}$ where

$$\partial^\bullet\eta := \eta_t + \boldsymbol{v}\cdot\nabla\eta \tag{2}$$

denotes the material derivative. Again observe that although this definition uses standard derivatives of η which may be obtained by using an extension of η off the surface, the material derivative only depends on values of η on the time dependent surface.

Combining the two equations results in

$$\int\limits_{\mathcal{R}(t)} \partial^\bullet u_i + u_i\nabla_\Gamma\cdot\boldsymbol{v} + \nabla_\Gamma\cdot\boldsymbol{q}_i = \int\limits_{\mathcal{R}(t)} f_i(\boldsymbol{u}).$$

Since $\mathcal{R}(t)$ is arbitrary for all time t, we conclude that

$$\partial^\bullet u_i + u_i\nabla_\Gamma\cdot\boldsymbol{v} + \nabla_\Gamma\cdot\boldsymbol{q}_i = f_i(\boldsymbol{u}), \quad \text{on } \Gamma(t). \tag{3}$$

For the constitutive law relating the flux to the concentrations, assuming no cross-diffusion between the chemical species, we set $\mathcal{D}$ to be a diffusivity tensor (a diagonal

matrix diffusion coefficients) and assume that the chemical species diffuse according to Fick's law

$$\boldsymbol{q}_i = -\mathcal{D}_{ij}\nabla_\Gamma u_j, \tag{4}$$

where $\mathcal{D}_{ij} = d_i\delta_{ij}$, with δ_{ij} representing the usual Kronecker delta function. Then (3) becomes

$$\partial^\bullet u_i + u_i\nabla_\Gamma \cdot \boldsymbol{v} = \nabla_\Gamma(\mathcal{D}_{ij}\nabla_\Gamma u_j) + f_i(\boldsymbol{u}), \quad \text{on } \Gamma(t).$$

In vector form, the system of reaction-diffusion equations on an evolving surface $\Gamma(t)$ takes the form

$$\partial^\bullet \boldsymbol{u} + \boldsymbol{u}\nabla_\Gamma \cdot \boldsymbol{v} = D\Delta_\Gamma \boldsymbol{u} + \boldsymbol{f}(\boldsymbol{u}), \tag{5}$$

where $D = diag(d_i)$. This system is supplemented with zero-flux boundary conditions if the boundary of $\Gamma(t)$ is non-empty and the initial conditions

$$\boldsymbol{u}(\cdot, 0) = \boldsymbol{u}_0(\cdot) \quad \text{on } \Gamma(0) \tag{6}$$

where the components of $\boldsymbol{u}_0(\cdot)$ are prescribed positive bounded functions.

Remark 1 Equation (5) is similar to the model investigated in Madzvamuse et al. (2005) for the planar case if we replace derivatives by tangential derivatives. Note that in the planar case there is no normal velocity and $\boldsymbol{v} = \boldsymbol{v}_T$.

Remark 2 Note that this derivation of the equation is for an arbitrary velocity field $\boldsymbol{v}$ which could depend on the surface $\Gamma(t)$ itself and the solutions of the reaction-diffusion system.

2.3 Illustrative models

– **Reaction kinetics**

For simplicity we focus in this paper on the development of patterns modelled by a two component system so that $\boldsymbol{u} = (u, w)$ where u and w are the concentrations of two chemical specimens. There are numerous models each of which leads to a particular form of the reaction terms f_1 and f_2 in (5). We refer to Maini et al. (1997) for a review of commonly used reaction kinetics and their motivation. For illustrative purposes we consider the *activator-depleted* substrate model (Gierer and Meinhardt 1972; Prigogine et al. 1968; Schnakenberg 1979) also known as the Brusselator model given by

$$\boldsymbol{f}(\boldsymbol{u}) = (f_1, f_2)^T = \Big(\gamma(a - u + u^2 w), \gamma(b - u^2 w)\Big)^T \tag{7}$$

where γ, a and b are positive constants. Observe that there is a unique solution to $\boldsymbol{f}(\boldsymbol{u}) = \boldsymbol{0}$ given by

$$u = a + b\,, \quad w = b/(a+b)^2 \tag{8}$$

which corresponds to a unique steady state of (5) on a stationary surface. For a given model, there may be a set of parameters, whose values belong to the Turing space, for which the model on fixed domains exhibits spatial pattern formation due to diffusion-driven instability of spatially uniform structures. For example on fixed domains, Murray (2002), summarises necessary conditions on the parameters a, b and d based on linear stability analysis for Turing diffusion-driven instability to occur for the case of the *activator-depleted* model.

Domain growth increases the range of biological morphogen pairings which have the potential to induce Turing patterning compared to a fixed domain (Madzvamuse 2009). It is now possible to suggest and investigate, for example, *activator-activator* or *short-range inhibition, long-range activation* as paradigms for biological pattern formation on growing domains. More generally, there exists a larger family of reaction kinetics capable of generating diffusively-driven instability patterns in the presence of domain growth (Madzvamuse 2009). Such models can be easily incorporated under the surface finite element formulation. In this paper we restrict our attention to (7).

- **Surface growth**
  We focus on three growth models for the evolution of the surface.
  - **Isotropic growth**
    Here we assume that each material point on the surface undergoes the same prescribed dilation so that if $X(t)$ denotes a material point on $\Gamma(t)$ then

$$X(t) = \rho(t) X_0 \tag{9}$$

    where the dilation factor $\rho(t)$ is a positive growth function satisfying the property that $\rho(0) = 1$. Note that in general such a surface growth involves both a normal velocity and a tangential velocity. However in the case of a sphere we may write

$$X(t) = \rho(t) R_0 \boldsymbol{\nu} \tag{10}$$

    where $\boldsymbol{\nu}$ is an arbitrary vector on the unit sphere so that the material velocity is

$$\boldsymbol{v}(X(t), t) = \dot{X} = V \boldsymbol{\nu}, \quad \text{with} \quad V = R_0 \dot{\rho}(t)$$

    and $\boldsymbol{\nu}$ is the unit normal to the evolving surface.
  - **Anisotropic growth**
    Here we are interested in a prescribed velocity law associated with non-isotropic growth. As an illustrative example we consider the following surface: let $\phi(x, t)$ be the prescribed level set function

$$\phi(x, t) = x_1^2 + x_2^2 + a(t)^2 G(x_3^2 / L(t)^2) - a(t)^2 \tag{11}$$

and the surface $\Gamma(t)$ be described by the zero level set of ϕ. Different surfaces may be obtained by prescribing the non-negative shape functions $G(\cdot)$, $a(\cdot)$ and $L(\cdot)$ with $G(0) = 0$ and $G(1) = 1$.

- *Tangential and normal motion*
  For the given surface, material points may move in the tangential as well as the normal direction. We set the surface $\Gamma(t)$ to comprise material points $(X(t), Y(t), Z(t))$ and parameterise in the following way: given $Z(0) \in [-L(0), L(0)]$ choose $(X(0), Y(0))$ to lie on the circle

$$X(0)^2 + Y(0)^2 = a(0)^2(1 - G(Z(0)^2/L(0)^2))$$

  and

$$Z(t) = Z(0)\frac{L(t)}{L(0)}, \quad X(t) = X(0)\frac{a(t)}{a(0)} \quad \text{and} \quad Y(t) = Y(0)\frac{a(t)}{a(0)} \tag{12}$$

  so that

$$\phi(X(t), Y(t), Z(t), t) = 0.$$

- *Normal motion*
  On the other hand we may choose material points on the same surface but such that the velocity of material points, $v(X(t), Y(t), Z(t))$, is in the normal direction

$$\boldsymbol{v}(x,t) = V(x,t)\boldsymbol{\nu}(x,t), \quad \boldsymbol{\nu}(x,t) = \frac{\nabla\phi(x,t)}{|\nabla\phi(x,t)|} \quad \text{and} \quad V(x,t) = -\frac{\phi_t(x,t)}{|\nabla\phi(x,t)|}.$$

– **Chemically-driven surface evolution**

We envisage that the complex mathematical models for pattern formation on evolving surfaces will couple the growth process to surface concentration of species (or chemical concentrations) leading to the law of the form

$$V = g(\boldsymbol{u}, \boldsymbol{\nu}, H) \tag{13}$$

for the normal velocity where H is the mean curvature of the surface. Here we use the definition of mean curvature to be the sum of the two principle curvatures (Deckelnick et al. 2005) and the convention that the mean curvature of a sphere is positive when the normal is oriented outwards of the ball. Actually one could consider more general laws in which other geometric quantities such as the Laplace–Beltrami operator acting on the mean curvature (Elliott and Stinner 2010). Equations such as (13) arise naturally when the surface is energetic (Deckelnick et al. 2005). In addition to (13) there may also be an equation for the tangential velocity. In this paper we focus on an example for which the motion is in the normal direction only.

3 Surface finite element method

In this section we present the surface finite element method applied to reaction-diffusion systems on evolving surfaces.

3.1 Variational formulation

For an arbitrary i

$$\partial^\bullet u_i + u_i \nabla_\Gamma \cdot \boldsymbol{v} = d_i \Delta_\Gamma u_i + f_i(\boldsymbol{u}). \tag{14}$$

Let $\varphi(\cdot, t) \in H^1(\Gamma(t))$ be a test function. Multiplying (14) by φ and integrating over $\Gamma(t)$ leads to

$$\begin{aligned}\int_{\Gamma(t)} f_i(\boldsymbol{u})\varphi &= \int_{\Gamma(t)} \partial^\bullet u_i \varphi + u_i \varphi \nabla_\Gamma \cdot \boldsymbol{v} - d_i \int_{\Gamma(t)} \varphi \Delta_\Gamma u_i \\ &= \int_{\Gamma(t)} \partial^\bullet u_i \varphi + u_i \varphi \nabla_\Gamma \cdot \boldsymbol{v} + d_i \int_{\Gamma(t)} \nabla_\Gamma u_i \cdot \nabla_\Gamma \varphi - \int_{\partial\Gamma(t)} \varphi \nabla_\Gamma u_i \cdot \boldsymbol{\mu}.\end{aligned} \tag{15}$$

The last term vanishes if $\partial\Gamma(t) = \emptyset$ or $\partial\Gamma(t) \neq \emptyset$ but $\varphi = 0$ or $\nabla_\Gamma u_i \cdot \boldsymbol{\mu} = 0$ on $\partial\Gamma(t)$. Hence, assuming any of these conditions holds we have

$$\begin{aligned}\int_{\Gamma(t)} f_i(\boldsymbol{u})\varphi &= \int_{\Gamma(t)} \partial^\bullet u_i \varphi + u_i \varphi \nabla_\Gamma \cdot \boldsymbol{v} + d_i \int_{\Gamma(t)} \nabla_\Gamma u_i \cdot \nabla_\Gamma \varphi \\ &= \int_{\Gamma(t)} \partial^\bullet (u_i \varphi) - u_i \partial^\bullet \varphi + u_i \varphi \nabla_\Gamma \cdot \boldsymbol{v} + d_i \int_{\Gamma(t)} \nabla_\Gamma u_i \cdot \nabla_\Gamma \varphi \\ &= \frac{d}{dt} \int_{\Gamma(t)} u_i \varphi - \int_{\Gamma(t)} u_i \partial^\bullet \varphi + d_i \int_{\Gamma(t)} \nabla_\Gamma \varphi \cdot \nabla_\Gamma u_i.\end{aligned} \tag{16}$$

The variational form seeks to find $u_i \in H^1(\Gamma(t))$ satisfying

$$\begin{aligned}&\frac{d}{dt} \int_{\Gamma(t)} u_i \varphi - \int_{\Gamma(t)} u_i \partial^\bullet \varphi + d_i \int_{\Gamma(t)} \nabla_\Gamma \varphi \cdot \nabla_\Gamma u_i \\ &\quad = \int_{\Gamma(t)} f_i(\boldsymbol{u})\varphi, \quad \forall \varphi \in H^1(\Gamma(t)).\end{aligned} \tag{17}$$

3.2 Evolving surface finite element method

We approximate $\Gamma(t)$ by $\Gamma_h(t)$, a triangulated surface whose vertices lie on $\Gamma(t)$, *i.e.* $\Gamma_h(t) = \mathcal{T}_h(t) = \bigcup_k T_k(t)$, where each $T_k(t)$ is a triangle. The diameter of the largest triangle in the initial surface is denoted by h. We choose the vertices of the triangulation to evolve with the material velocity so that

$$\dot{X}_j(t) = \boldsymbol{v}(X_j(t), t) \tag{18}$$

and it is easy to see that $X_j(t)$ lies on $\Gamma(t)$ if $\boldsymbol{v}$ is the exact material velocity. We assume $\Gamma_h(t)$ is smooth in time. For each t we define a finite element space

$$S_h(t) = \left\{ \phi \in C^0(\Gamma_h(t)) : \left. \phi \right|_{T_k} \text{ is linear affine for each } T_k \in \mathcal{T}_h(t) \right\}.$$

For each $t \in [0, T]$ we denote by $\{\chi_j(\cdot, t)\}_{j=1}^N$ the moving nodal basis functions and by $X_j(t),\ j = 1, \ldots, N$ the nodes. These functions will satisfy

$$\chi_j(\cdot, t) \in C^0(\Gamma_h(t)), \quad \chi_j(X_i(t), t) = \delta_{ij}, \quad \left. \chi_j(\cdot, t) \right|_{T_k} \text{ is linear affine,}$$

and on $T_k \in \mathcal{T}_h(t)$

$$\left. \chi_j \right|_e = \lambda_k, \quad \text{for each } e \in \mathcal{T}_h(t)$$

where $k = k(T_k, j)$ and $(\lambda_1, \lambda_2, \lambda_3)$ are the barycentric coordinates.

On $\Gamma_h(t)$ we define the discrete material velocity

$$\boldsymbol{v}_h = \sum_{j=1}^{N} \dot{X}_j(t) \chi_j \tag{19}$$

and the discrete material derivative

$$\partial_h^\bullet \phi = \phi_t + v_h \cdot \nabla \phi. \tag{20}$$

Proposition 1 (Transport property) *On $\Gamma_h(t)$, for each $j = 1, \ldots, N$,*

$$\partial_h^\bullet \chi_j = 0$$

and for each $\phi = \sum_{j=1}^N \gamma_j(t) \chi_j \in S_h(t)$ then $\partial_h^\bullet \phi = \sum_{j=1}^N \dot{\gamma_j}(t) \chi_j$.

Proof See Dziuk and Elliott (2007a). □

We seek approximations $U_i(\cdot, t) \in S_h(t)$ to u_i, for $i = 1, 2$. Since $\{\chi_j(\cdot, t)\}_{j=1}^N$ is the basis of $S_h(t)$ we know for each $U_i(\cdot, t) \in S_h(t)$ and each $t \in [0, T]$ that there

exist unique $\boldsymbol{\alpha_i} = \left\{\alpha_i^1(t), \ldots, \alpha_i^N(t)\right\}$ satisfying

$$U_i(\cdot, t) = \sum_{j=1}^{N} \alpha_i^j(t)\chi_j(\cdot, t).$$

Substituting $U_i(\cdot, t)$, $\Gamma_h(t)$ and $\phi \in S_h(t)$ for u_i, $\Gamma(t)$ and φ in (17) we obtain

$$\frac{d}{dt}\int_{\Gamma_h(t)} \sum_{j=1}^{N} \alpha_{i,t}^j \chi_j \phi - \int_{\Gamma(t)} \sum_{j=1}^{N} \alpha_{i,t}^j \chi_j \partial_h^\bullet \phi + \int_{\Gamma_h(t)} \sum_{j=1}^{N} \alpha_1^j \chi_j \phi \nabla_{\Gamma_h} \cdot \boldsymbol{v}_h$$
$$+ d_i \int_{\Gamma_h(t)} \sum_{j=1}^{N} \alpha_i^j(t) \nabla_{\Gamma_h} \chi_j \cdot \nabla_{\Gamma_h(t)} \phi = \int_{\Gamma_h} f_1 \phi, \tag{21}$$

for all $\phi \in S_h(t)$ and taking $\phi = \chi_k$, $k = 1, \ldots, N$ and using the transport property of the basis functions we obtain

$$\frac{d}{dt}\left(\mathcal{M}(t)\boldsymbol{\alpha}_i\right) + d_i \mathcal{S}(t)\boldsymbol{\alpha}_i = \boldsymbol{F}_i(t) \tag{22}$$

where $\mathcal{M}(t)$ is the evolving mass matrix

$$\mathcal{M}(t)_{jk} = \int_{\Gamma_h(t)} \chi_j \chi_k,$$

$\mathcal{S}(t)$ is the evolving stiffness matrix

$$\mathcal{S}(t)_{jk} = \int_{\Gamma_h(t)} \nabla_{\Gamma_h} \chi_j \cdot \nabla_{\Gamma_h} \chi_k$$

and $\boldsymbol{F}_i$ is the right hand side $\boldsymbol{F}_{ij} = \int_{\Gamma_h(t)} f_i(\boldsymbol{U})\chi_j$.

Remark 3 The simple form of the system (22) is a consequence of the evolution of triangle vertices by the material velocity (18). This is a Lagrangian discretisation.

3.3 Time discretization

For simplicity we restrict the description to the two component system $\boldsymbol{u} = (u, w)$ with kinetics given by (7) and $d_1 = 1, d_2 = d$. We discretise in time using a uniform time step τ. We represent by (U^n, W^n) the solution at time $n\tau$ and $\Gamma^n = \Gamma(n\tau)$. Let

$U^0, W^0 \in S_h(0)$ be given. For $n = 0, \ldots, n_T$, solve the nonlinear system

$$\begin{cases} \frac{1}{\tau} \int\limits_{\Gamma_h^{n+1}} U^{n+1} \chi_j^{n+1} + \int\limits_{\Gamma_h^{n+1}} \nabla_{\Gamma_h^n} U^{n+1} \cdot \nabla_{\Gamma_h^n} \chi_j^{n+1} \\ \quad = \frac{1}{\tau} \int\limits_{\Gamma^n} U^n \chi_j^n + \int\limits_{\Gamma_h^{n+1}} f_1\left(U^{n+1}, W^{n+1}\right) \chi_j^{n+1}, \\ \\ \frac{1}{\tau} \int\limits_{\Gamma_h^{n+1}} W^{n+1} \chi_j^{n+1} + d \int\limits_{\Gamma_h^{n+1}} \nabla_{\Gamma_h^n} W^{n+1} \cdot \nabla_{\Gamma_h^n} \chi_j^{n+1} \\ \quad = \frac{1}{\tau} \int\limits_{\Gamma^n} W^n \chi_j^n + \int\limits_{\Gamma_h^{n+1}} f_2\left(U^{n+1}, W^{n+1}\right) \chi_j^{n+1}, \end{cases} \tag{23}$$

for all $j = 1, \ldots, N$. To linearise $f_1\left(U^{n+1}, W^{n+1}\right)$ we assume slow deformation of the evolving surface which allows us to write $\left(U^{n+1}\right)^2 \approx U^n U^{n+1}$ (Madzvamuse 2006).

Using this linearisation, we can derive the following fully discrete algorithm:

Let $U^0, W^0 \in S_h(0)$ be given. For $n = 0, \ldots, n_T$ solve the linear system

$$\begin{cases} \left(\frac{1}{\tau} + \gamma\right) \int\limits_{\Gamma_h^{n+1}} U^{n+1} \chi_j^{n+1} + \int\limits_{\Gamma_h^{n+1}} \nabla_{\Gamma_h^n} U^{n+1} \cdot \nabla_{\Gamma_h^n} \chi_j^{n+1} \\ \quad -\gamma \int\limits_{\Gamma_h^{n+1}} U^n W^n U^{n+1} \chi_j^{n+1} = \frac{1}{\tau} \int\limits_{\Gamma^n} U^n \chi_j^n + \gamma a \int\limits_{\Gamma_h^n} \chi_j^n, \\ \\ \frac{1}{\tau} \int\limits_{\Gamma_h^{n+1}} W^{n+1} \chi_j^{n+1} + d \int\limits_{\Gamma_h^{n+1}} \nabla_{\Gamma_h^n} W^{n+1} \cdot \nabla_{\Gamma_h^n} \chi_j^{n+1} \\ \quad +\gamma \int\limits_{\Gamma_h^{n+1}} \left(U^{n+1}\right)^2 W^{n+1} \chi_j^{n+1} = \frac{1}{\tau} \int\limits_{\Gamma^n} W^n \chi_j^n + \gamma b \int\limits_{\Gamma_h^n} \chi_j^n, \end{cases} \tag{24}$$

for all $j = 1, \ldots, N$. Using a matrix representation we have,

$$\begin{cases} \left(\left(\frac{1}{\tau} + \gamma\right) \mathcal{M}^{n+1} + \mathcal{S}^{n+1} - \gamma \mathcal{M}_1^{n+1}\right) \boldsymbol{U}^{n+1} = \frac{1}{\tau} \mathcal{M}^n \boldsymbol{U}^n + \boldsymbol{F}_1^n, \\ \left(\frac{1}{\tau} \mathcal{M}^{n+1} + d\mathcal{S}^{n+1} + \gamma \mathcal{M}_2^{n+1}\right) \boldsymbol{W}^{n+1} = \frac{1}{\tau} \mathcal{M}^n \boldsymbol{W}^n + \boldsymbol{F}_2^n, \end{cases} \tag{25}$$

with

$$\begin{aligned} \mathcal{M}_{ij}^n &= \int\limits_{\Gamma_h^n} \chi_i^n \chi_j^n, \quad \mathcal{M}_{1\,ij}^n = \int\limits_{\Gamma_h^n} U^n W^n \chi_i^n \chi_j^n, \quad \mathcal{M}_{2\,ij}^n = \int\limits_{\Gamma_h^n} \left(U^{n+1}\right)^2 \chi_i^n \chi_j^n, \\ \mathcal{S}_{ij}^n &= \int\limits_{\Gamma_h^n} \nabla_{\Gamma_h^n} \chi_i^n \cdot \nabla_{\Gamma_h^n} \chi_j^n, \quad \boldsymbol{F}_{1\,i}^n = \gamma a \int\limits_{\Gamma_h^n} \chi_i^n, \qquad \boldsymbol{F}_{2\,i}^n = \gamma b \int\limits_{\Gamma_h^n} \chi_i^n, \end{aligned} \tag{26}$$

where $\chi_i^n \in S_h^n = \left\{\chi \in C^0\left(\Gamma_h(n\tau)\right) : \ \chi_j\big|_e \ \text{ is linear affine for each } e \in \mathcal{T}_h(n\tau)\right\}$.

Remark 4 The method requires a triangulation of the initial surface. For example, the sphere is triangulated in the following way. A very coarse triangulation is obtained by hand using 6 points placed uniformly on the sphere. This triangulation is then successively refined uniformly by subdividing each triangle into two. New vertices are then projected onto the surface of the sphere. This process is implemented in ALBERTA which requires an algorithm for the projection of a point onto the surface which is readily available for a sphere. This refinement is repeated until an acceptable maximum mesh size is obtained.

Remark 5 We observe that various convergence results and error bounds have been proved for the surface finite element. See Dziuk (1988); Dziuk and Elliott (2007a,b, 2010) and the references cited therein.

4 Turing patterns

4.1 Turing patterns on fixed surfaces

As mentioned earlier we focus on the kinetics (7) with $d_1 = 1$ and $d_2 = d$. We begin by describing some simulations on a fixed surface. We choose the surface to be a sphere and fix the parameters a, b and d whilst varying γ. We also investigate the effect of refining the mesh for one of the examples.

4.1.1 The effect of varying γ

We use the following parameters: for the kinetics $a = 0.1$, $b = 0.9$ and for the diffusion coefficient, $d = 10$. Initial conditions are taken as small random perturbations around the homogeneous state $(1, 0.9)$ which is a steady state for a stationary surface. Notice that this choice of parameter values satisfy the conditions necessary for diffusion-driven instability on a fixed surface. Hence, we use the same parameters as (Madzvamuse 2006) on a static unit sphere in three simulations in which we vary only γ (see Table 1) in order to observe its effect on patterning. We point out that the initial conditions used were exactly the same for the three experiments. The results for the concentrations u and w at $t = 10$ are displayed in Fig. 1. The colours red and orange represent high values in concentration while blue represents lower values.

As we can see in Fig. 1, the effect of varying γ while keeping all other parameters fixed is that the complexity of the pattern increases as γ increases. It must be noted that γ represents the scale length, increasing γ is equivalent to increasing surface size. The

Table 1 Parameters used to simulate reaction-diffusion Eq. (5) on the unit sphere

Experiment	d	$\boldsymbol{\gamma}$	a	b	h	Timestep	End time
1	10	**30**	0.1	0.9	0.055	0.001	10
2	10	**200**	0.1	0.9	0.055	0.001	10
3	10	**500**	0.1	0.9	0.055	0.001	10

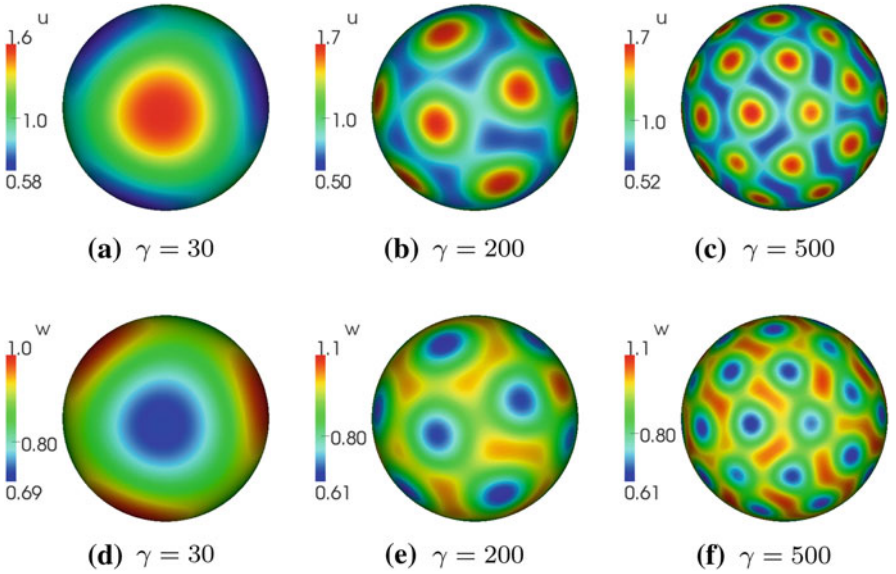

Fig. 1 Colour version online: concentration values u and w on a unit sphere at $t = 10$ for the choices $a = 0.1$, $b = 0.9$, $d = 10$ and $\gamma = 30, 200, 500$. *Red* and *orange* colours represent high values in concentration while blue represent lower values

same effect was observed in the numerical computations presented in Madzvamuse and Maini (2007) and Chaplain et al. (2001) for example, although in this last one the parameter values for a, b and d are different from the ones used in our work. Notice that regions with high values of u correspond to low values of w and vice versa, i.e. the solution profiles of u and w are in opposite phase. From now onward we show only solutions profiles corresponding to the concentration u.

4.1.2 The effect of mesh refinement

Here we demonstrate that the discretisation is accurate and robust by simulating the above example with $\gamma = 200$ using different triangulations. An initial triangulation of the sphere with $h \approx 0.055$ is uniformly refined twice by reducing the mesh size by a factor of 2. The time step is also refined by a factor of 2. All other parameter values are held constant. The initial concentration is generated by a random perturbation around the uniform steady state. Thus in order to compare solutions the simulations for the two refined meshes use an interpolation of the solution for the initial coarse mesh at $t = 0.1$. In Table 2 we present the parameters used for each simulation. We observe in Fig. 2 that the patterns are robust and quantitatively similar as h is varied. Also in Fig. 3 we display the evolution of the maximum and minimum values that the discrete solution u attains on the sphere as a function of time for each simulation. The graphs indicate convergence as the mesh sizes decrease.

Table 2 Parameters used for numerically solving the reaction-diffusion system (5) on a unit sphere using three different triangulations

h	Elements	γ	a	b	Timestep
0.0723	16384	200	0.1	0.9	2×10^{-3}
0.0550	32768	200	0.1	0.9	1×10^{-3}
0.0362	65536	200	0.1	0.9	5×10^{-4}

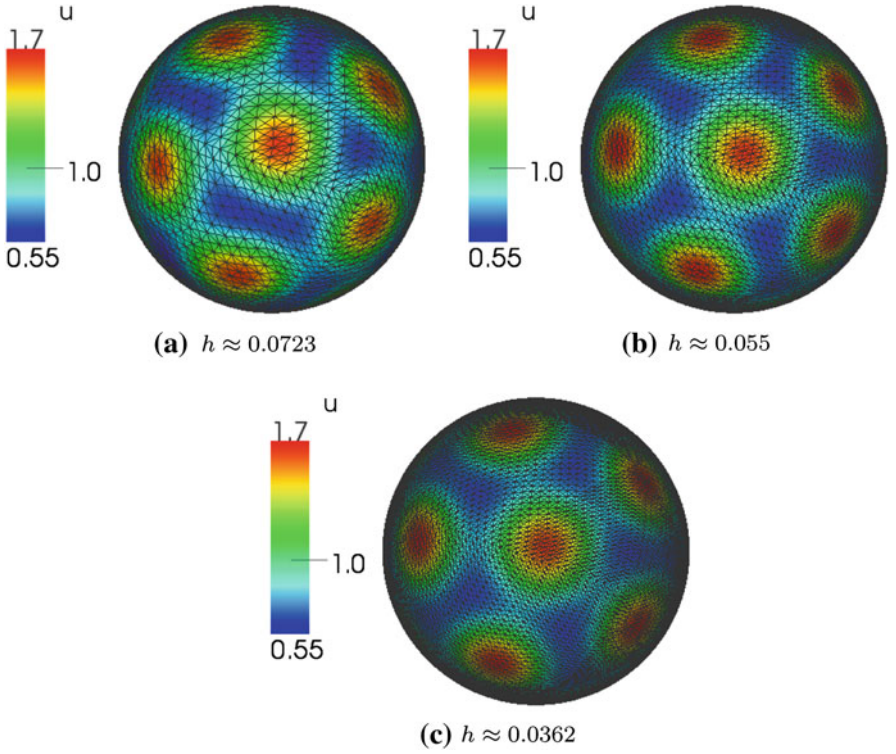

Fig. 2 Colour version online: concentration values u obtained at $t = 10$ using three different triangulations as shown in Table 2

4.2 Turing patterns on evolving surfaces

To demonstrate the applicability, flexibility, versatility and generality of our ESFEM we illustrate in this section two different scenarios describing surface evolution. The first example is that of an evolving sphere which grows at a logistic rate; that is the radius of the sphere grows exponentially in the initial stages and then saturates to a limiting finite fixed value at later stages of growth. This growth profile is plausible from the biological perspective since all organisms grow to a finite fixed size during the later stages of growth. Other types of isotropic growth profiles such as exponential or linear can be easily treated in this framework. Our second example demonstrates the generality of our method by dealing with non-isotropic growth.

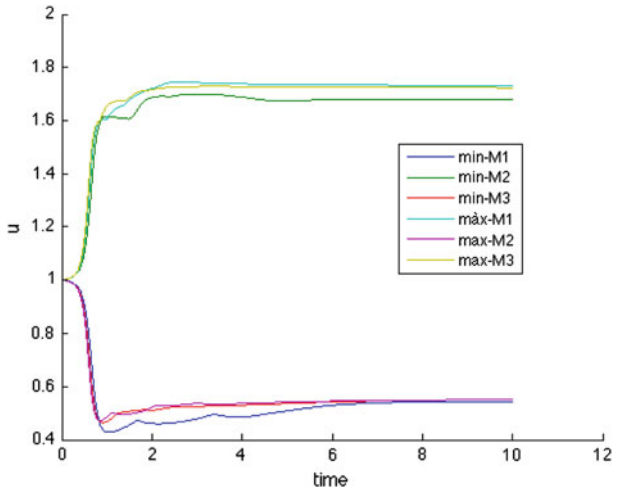

Fig. 3 Colour version online: evolution of minimum and maximum values of u for each of the three triangulations. M1 is the coarser mesh (16384 elements), M3 is the most refined one (65536 elements)

4.2.1 Example 1: Logistic growth

For illustrative purposes we consider an evolving sphere given by (10) with initial unit radius. The sphere evolves according to the logistic growth function $\rho(t)$ defined by

$$\rho(t) = \frac{e^{rt}}{1 + \frac{1}{K}(e^{rt} - 1)}, \tag{27}$$

where $r > 0$ and $K > 1$. Here r is the growth rate of the surface and K is the limiting final fixed size of the radius.

Figure 4 illustrates transient numerical solutions corresponding to the u concentration on an evolving sphere whose growth is defined by (27). Initial conditions are taken as small random perturbations around the uniform steady state (1.0, 0.9). Snapshot transient solutions are captured at times $t = 10$, 30 and 50 where the sphere

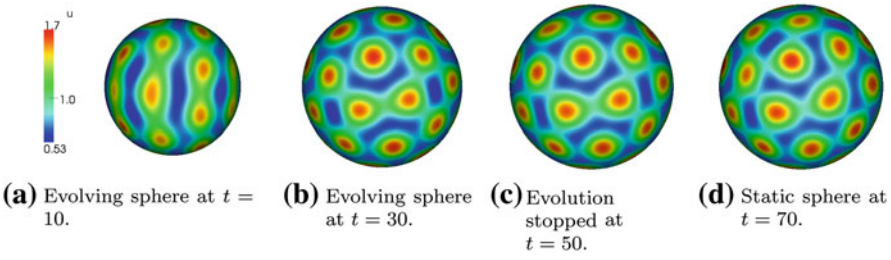

(a) Evolving sphere at $t = 10$. **(b)** Evolving sphere at $t = 30$. **(c)** Evolution stopped at $t = 50$. **(d)** Static sphere at $t = 70$.

Fig. 4 Colour version online: numerical results illustrating the transient solutions corresponding to the u concentration on a continuously evolving sphere defined by (10). The sphere evolves according to the logistic growth function (27). Model and numerical parameter values are given in Table 3

Table 3 Parameters used for reaction-diffusion simulation on a surface growing according to logistic growth

d	γ	a	b	K	r	Timestep	Solver	Solver Tol.
10	200	0.1	0.9	1.5	0.1	5×10^{-4}	GMRes	10^{-9}

is continuously evolving. At time $t = 50$, surface evolution is switched-off and the solutions are allowed to evolve to an inhomogeneous steady state on the final static sphere. The solution at time $t = 70$ appears to be a re-orientation (through rotation) of the transient solution at time $t = 50$.

We now consider the model equations on a static sphere whose radius is obtained from the logistic growth function at time $t = 50$. For this numerical experiment, initial conditions at time $t = 0$ are taken as small random perturbations around the uniform steady state as above. In Fig. 5 we illustrate the evolution of the inhomogeneous steady state in the absence of surface evolution. A detailed bifurcation analysis on evolving surfaces is warranted in order to understand the differences between the patterns in Fig. 4d and Fig. 5d and this is the subject of current studies.

4.2.2 Example 2: Anisotropic growth

Figure 6 illustrates the results of the implementation of the ESFEM applied to the reaction-diffusion system (5) where the surface $\Gamma(t)$ is given by (11) and (12) with the shape functions being

$$\begin{cases} L(t) &= \frac{L_0}{\beta+(1-\beta)e^{-rt}}, \\ a(t) &= a_0\left(1+\alpha(1-e^{-kt})\right), \\ G(s) &= s^{2p}, \end{cases} \tag{28}$$

where $L_0 = 0.5$, $a_0 = 0.1$, $\alpha = 0.8$, $\beta = 0.3$, $r = 0.5$, $k = 0.5$ and $p = 5$. The rest of the parameters are listed in Table 4. Initial conditions are prescribed to be small random perturbations around the uniform steady state obtained on a fixed surface.

We use a triangulation of the initial surface with 32700 elements and such that the largest triangle diameter is $h \approx 0.0215$. The initial triangulation was obtained using a C package Gnu triangulated surfaces (GTS) (http://gts.sourceforge.net/).

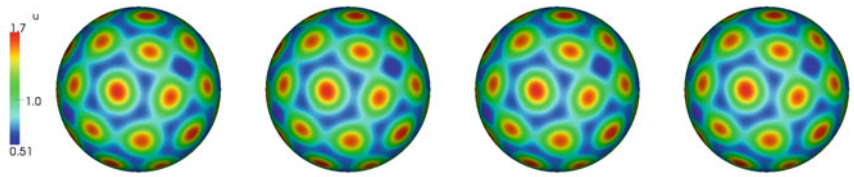

(a) Static sphere at $t = 10$. **(b)** Static sphere at $t = 30$. **(c)** Static sphere at $t = 50$. **(d)** Static sphere at $t = 70$.

Fig. 5 Colour version online: numerical results illustrating the spatially inhomogeneous solutions corresponding to the u concentration on a static sphere of radius approximately 1.5 (the limiting radius of the logistic growth function). Model and numerical parameter values are given in Table 3

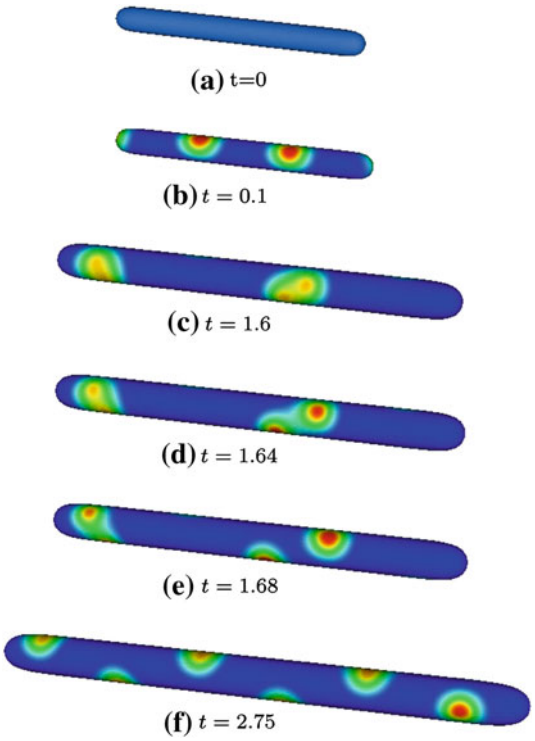

Fig. 6 Colour version online: numerical transient solutions corresponding to the u concentration values at times $t = 0, 0.1, 1.6, 1.64, 1.68$ and 2.75 on a surface evolving according to anisotropic growth defined by equations (11) and (28)

Table 4 Parameters used for reaction-diffusion simulation on an evolving surface (anisotropic growth)

d	γ	a	b	Timestep	Solver	Solver Tol.
100	500	0.1	0.9	5×10^{-4}	GMRes	10^{-9}

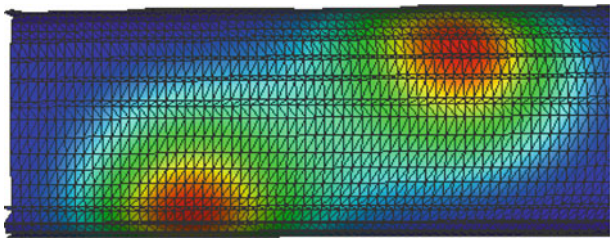

Fig. 7 Colour version online: detail of the mesh surrounding a breaking spot (at $t = 1.64$) for the pattern formation on a surface evolving according to anisotropic growth

Figure 6 illustrates the results of our simulation with model parameter values in Table 4. Initially no patterns are observed, then spot-period doubling bifurcation starts to emerge with further evolution of the surface. Period doubling in spots occurs through peak splitting, a process studied in Crampin et al. (2002). Furthermore, similar bifurcation sequences were observed on two-dimensional growing domains with exponential growth, see Madzvamuse and Maini (2007). In Fig. 7 detail of the mesh surrounding

a breaking spot is shown. It is clear that there is enough refinement to resolve the interface between higher and lower concentration regions.

5 Pre-pattern theory applied to the growth of solid tumours

In this section we illustrate the application of ESFEM to a system coupling surface evolution with surface reaction-diffusion by considering a model for tumour growth. It is not our purpose to go deep into the biological motivation for the model of tumour growth or give an extensive background. We refer to Chaplain et al. (2001) for an overview and provide just a brief description. We begin with a description of the model, followed by a description of the numerical approach and finally present some numerical simulations.

5.1 Model formulation

The model comprises the reaction-diffusion system (5) with activator-depleted kinetics of the form (7) and surface growth law of the form (13). Here u denotes the growth-promoting factor and w denotes the growth-inhibiting factor (Crampin et al. 1999). Furthermore, we consider the surface evolution to be governed by the normal velocity of the form

$$V = \delta u - \epsilon H \tag{29}$$

where δ is a growth rate and ϵ may be considered to be a parameter which models the surface tension of the tumour surface. We may also view ϵ as a small mathematical parameter which regularises the evolution law. This is useful because it is easy to see that even in the simple case of the surface velocity being constant in the normal direction it is possible for smooth surfaces to develop corners in a short time.

Note that (29) is an equation for forced mean curvature flow of a surface (Dziuk and Elliott 2010). In the paper (Chaplain et al. 2001) numerical simulations of the reaction-diffusion system were carried-out on a stationary sphere in a pre-patterning stage and then the solution was used to show how the surface might grow initially in preferred directions with a model such as (29) for $\epsilon = 0$. The numerical method of Chaplain et al. (2001) applied was based on the method of lines with spherical harmonics. An advantage of ESFEM is that we only need the positions of the triangle vertices in order to compute, resulting in an attractive flexibility of the method.

5.2 Numerical method

The numerical algorithm consists of two steps: given Γ_h^n, $\boldsymbol{X}^n$, $\boldsymbol{U}_h^n \in S_h^n$ find $\boldsymbol{X}^{n+1}$ and $\boldsymbol{U}_h^{n+1}$ by solving:

1.

$$\left(\frac{1}{\tau}\mathcal{M}^n + \epsilon\mathcal{S}^n\right) X^{n+1} = \frac{1}{\tau}\mathcal{M}X^n + G^n, \tag{30}$$

where X^n denotes the nodal coordinates at time n and $\mathcal{M}^n$ and $\mathcal{S}^n$ are block mass and stiffness matrices whose blocks are determined by the mass and stiffness matrices for the triangulated surface Γ_h^n, respectively, and

$$G_i^n = \int_{\Gamma^n} \delta(U_h^n)_1 v^n \chi_i. \tag{31}$$

Here the normal v^n is computed separately for each face of the triangle.

2. The newly computed coordinates of the triangle vertices X^{n+1} are used to calculate the mass and stiffness matrices at time level $n+1$. Then the following system

Table 5 Parameters used in the simulation of tumour growth

d	γ	a	b	$\bar{t}$	δ	ϵ	Timestep	Solver	Solver Tol.
10	30	0.1	0.9	5.	0.1	0.01	0.001	GMRes	10^{-9}

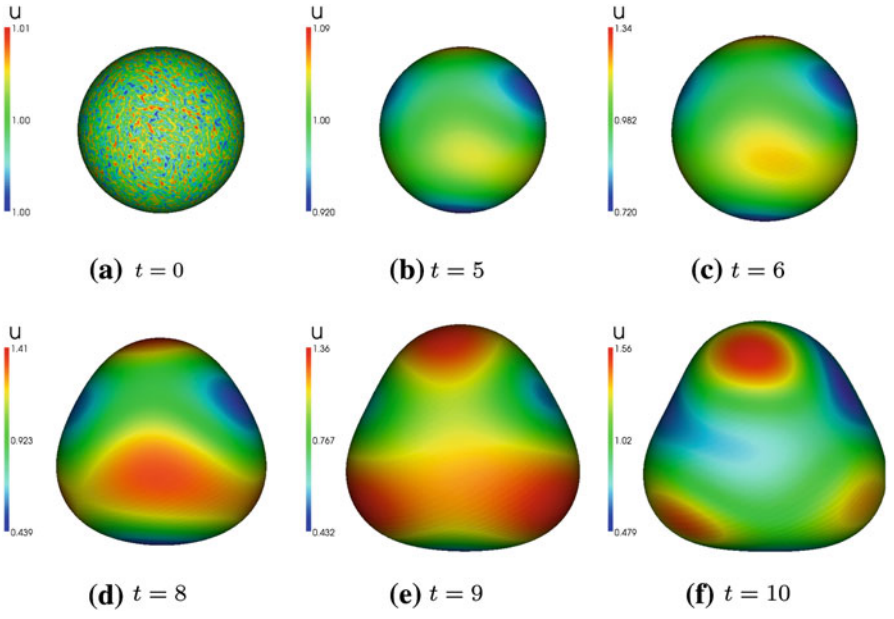

(a) $t = 0$ **(b)** $t = 5$ **(c)** $t = 6$

(d) $t = 8$ **(e)** $t = 9$ **(f)** $t = 10$

Fig. 8 Colour version online: concentration of the growth factor u for the tumour model with $\gamma = 30$

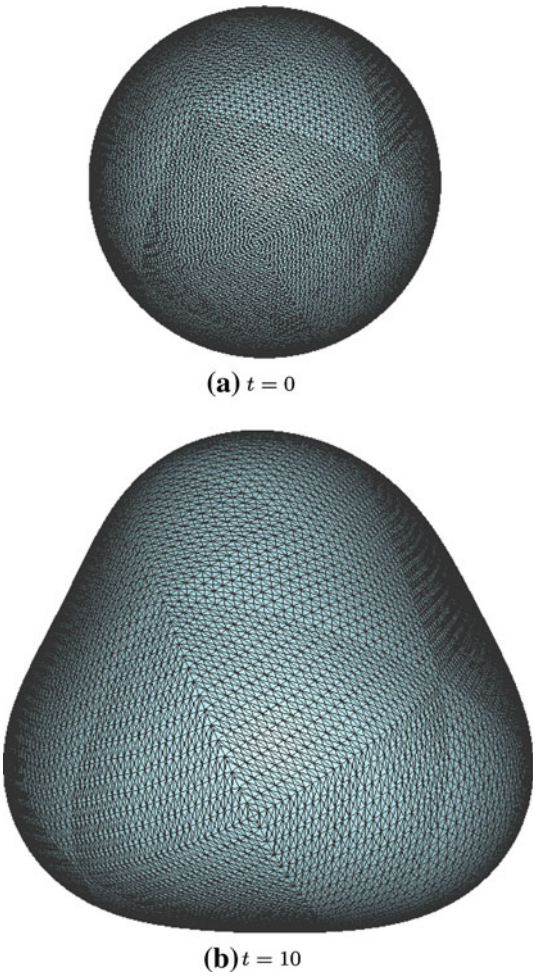

Fig. 9 Colour version online: initial and final triangulation for the example of tumour model with ($\gamma = 30$)

(recalling (25)) is solved:

$$\begin{cases} \left(\left(\frac{1}{\tau}+\gamma\right)\mathcal{M}^{n+1}+\mathcal{S}^{n+1}-\gamma\mathcal{M}_1^{n+1}\right)\boldsymbol{U}^{n+1}=\frac{1}{\tau}\mathcal{M}^n\boldsymbol{U}^n+\boldsymbol{F}_1^n, \\ \left(\frac{1}{\tau}\mathcal{M}^{n+1}+d\mathcal{S}^{n+1}+\gamma\mathcal{M}_2^{n+1}\right)\boldsymbol{W}^{n+1}=\frac{1}{\tau}\mathcal{M}^n\boldsymbol{W}^n+\boldsymbol{F}_2^n. \end{cases} \tag{32}$$

5.3 Numerical results

The parameter values have been chosen to illustrate the effectiveness of ESFEM in handling a problem for which the evolution of the surface depends on the solution of the surface reaction-diffusion system. Initial conditions are prescribed as small random perturbations around the homogeneous state $(u(\cdot,0), w(\cdot,0)) = (1.0, 0.9)$. The initial surface is the unit sphere and this is approximated using a triangulation

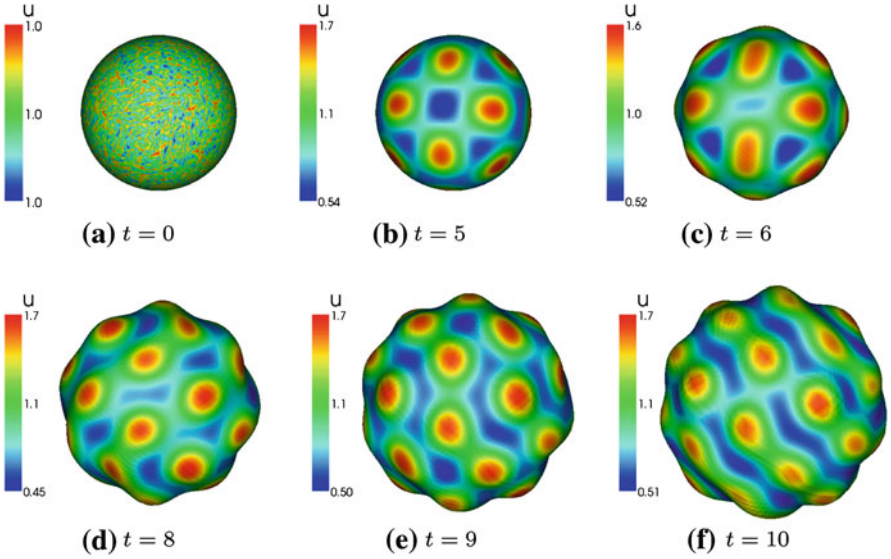

Fig. 10 Colour version online: concentration of the growth factor u for the tumour model with $\gamma = 200$

with 32768 elements for which $h \approx 0.055$. The rest of the parameters are given in Table 5.

In Fig. 8 we show a few snap-shots of the simulation of tumour growth by showing at the indicated times the tumour surface patterned by the concentration of the growth factor u. As expected we observe that regions of higher values of u correspond to regions of higher growth evolution of the surface.

More complex structures for the tumour surface are obtained by increasing the value of γ. This is a consequence of the increase in complexity of the patterns of u on the surface. Results are presented in Fig. 10 where all the parameters are the same as in Table 5 apart from the change of γ from 30 to 200. The initial and final triangulations are displayed in Fig. 11.

5.3.1 Mesh adaptivity and remeshing

In principle after some time, since the vertices of triangles evolve according to the velocity law, it is possible that triangulations of evolving surfaces may not be appropriate for the simulation. For example they could degenerate in the sense of the appearance of very small angles. On the other hand the triangulation may not resolve the features of the solution in subdomains where the concentrations change rapidly. It is also possible that the topology of the surface could change as a consequence of pinching-off and self-intersection. In the simulations presented in this paper a suitably uniformly refined initial triangulation was sufficient for the calculations. As can be seen from the depicted final triangulations the evolving surfaces were adequately approximated.

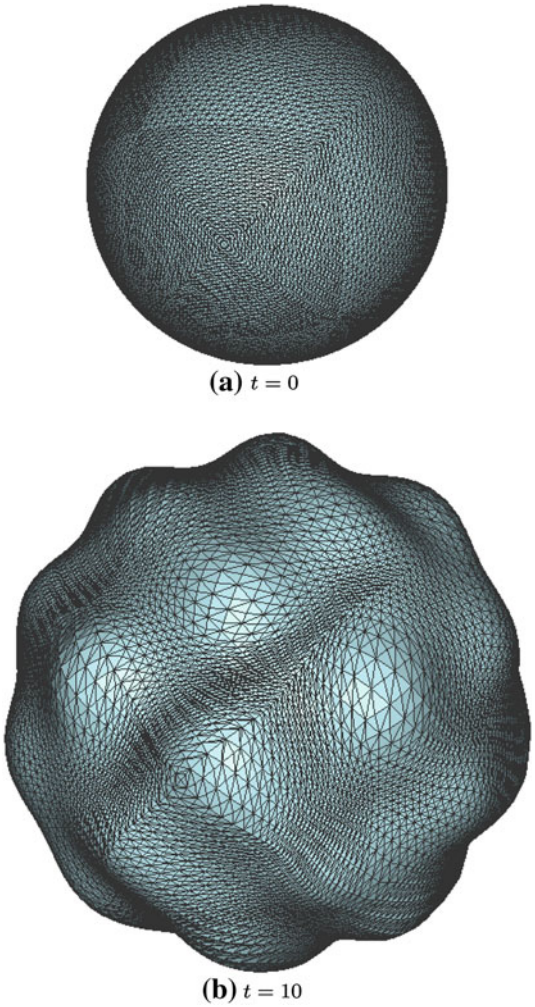

Fig. 11 Colour version online: initial and final triangulation for the example of tumour growth ($\gamma = 200$)

More efficient calculations can be carried out by refining and coarsening the triangulations in an adaptive way to reflect the behaviour of the solution of the surface partial differential equation and to avoid the degeneration of triangulations. We refer the reader to Barrett et al. (2008); Eilks and Elliott (2008); Elliott and Stinner (2010) for computational approaches to these issues.

6 Conclusion

The computations in this article illustrate the generality and applicability of the surface finite element method for solving nonlinear complex partial differential equations on evolving surface. In particular it provides computational biologists with a robust,

stable, accurate and a highly flexible method to model arbitrary surface evolution. Future developments should include:

- Adaptivity and remeshing.
- Application to complex models.
- Development of methods for surface topology change.
- Systematic study of particular systems.
- Linkage to solutions of equations holding in bulk domains.
- Bifurcation analysis on evolving surfaces.

Acknowledgments Part of RB's research was carried out at the Department of Mathematics of the University of Sussex supported by a Graduate Teaching Assistantship. RB has also used the computational resources of the Center for Mathematics and Fundamental Applications of the University of Lisbon. AM would like to acknowledge grant financial support from the LMS (*R4P2*), EPSRC (*EP/H020349/1*), the Royal Society Travel grant (*R4K1*) and the Royal Society Research Grant (*R4N9*). The research of CME has been supported by the UK Engineering and Physical Sciences Research Council (EPSRC), Grant EP/G010404.

References

Aragón JL, Barrio RA, Varea C (1999) Turing patterns on a sphere. Phys Rev E 60:4588–4592

Barreira R (2009) Numerical solution of non-linear partial differential equations on triangulated surfaces, D.Phil Thesis, University of Sussex

Barrett JW, Garcke H, Nürnberg (2008) Parametric approximation of Willmore flow and related geometric evolution equations. SIAM J Sci Comput 31:225–253

Barrio RA, Maini PK, Padilla P, Plaza RG, Sánchez-Garduno F (2004) The effect of growth and curvature on pattern formation. J Dyn Diff Equ 4:1093–1121

Calhoun DA, Helzel C (2009) A finite volume method for solving parabolic equations on logically cartesian curved surface meshes. SIAM J Sci Comput 6:4066–4099

Chaplain MAJ, Ganesh M, Graham IG (2001) Spatio-temporal pattern formation on spherical surfaces: numerical simulation and application to solid tumour growth. J Math Biol 42:387–423

Crampin EJ, Gaffney EA, Maini PK (2002) Mode doubling and tripling in reation-diffusion patterns on growing domains: a piecewise linear model. J Math Biol 44:107–128

Crampin EJ, Gaffney EA, Maini PK (1999) Reaction and diffusion on growing domains: scenarios for robust pattern formation. Bull Math Biol 61:1093–1120

Deckelnick KP, Dziuk G, Elliott CM (2005) Computation of Geometric PDEs and Mean Curvature Flow. Acta Numerica 14:139–232

Dziuk G (1988) Finite Elements for the Beltrami operator on arbitrary surfaces. Lecture Notes in Mathematics, Partial differential equations and calculus of variations, vol 1357. Springer, Berlin, pp 142–155

Dziuk G, Elliott CM (2007) Finite elements on evolving surfaces. IMA J Num Anal 27:262–292

Dziuk G, Elliott CM (2007) Surface finite elements for parabolic equations. J Comp Math 25:430–439

Dziuk G, Elliott CM (2010) An Eulerian approach to transport and diffusion on evolving surfaces. Comput Vis Sci 13:17–28

Dziuk G, Elliott CM (2010) L^2 estimates for the evolving surface finite element method. Math Comp (submitted)

Eilks C, Elliott CM (2008) Numerical simulation of dealloying by surface dissolution via the evolving surface finite element method. J Comp Phys 227:9727–9741

Elliott CM, Stinner B (2010) Modeling and computation of two phase geometric biomembranes using surface finite elements. J Comp Phys 229:6585–6612

Elliott CM, Stinner B, Styles VM (2010) Numerical computation of advection and diffusion on evolving diffuse interfaces. IMA J Num Anal. Advance Access published on 11 May 2010. doi:10.1093/imanum/drq005

Gierer A, Meinhardt H (1972) A theory of biological pattern formation. Kybernetik 12:30–39

Golub GH, Van Loan CF (1996) Matrix Computations. JHU Press, Baltimore

Greer J, Bertozzi AL, Sapiro G (2006) Fourth order partial differential equations on general geometries. J Comput Phys 216:216–246

Kondo S, Asai R (1995) A reaction-diffusion wave on the skin of the marine anglefish, Pomacanthus. Nature 376:765–768

Lefevre J, Mangin J-F (2010) A reaction-diffusion model of the human brain development. PLoS Comput Biol 6:e1000749

Madzvamuse A, Maini PK, Wathen AJ (2003) A moving grid finite element method applied to a model biological pattern generator. J Comp Phys 190:478–500

Madzvamuse A, Wathen AJ, Maini PK (2005) A moving grid finite element method for the simulation of pattern generation by Turing models on growing domains. J Sci Comp 24(2):247–262

Madzvamuse A (2006) Time-stepping schemes for moving grid finite elements applied to reaction-diffusion systems on fixed and growing domains. J Comput Phys 216:239–263

Madzvamuse A, Maini P (2007) Velocity-induced numerical solutions of reaction-diffusion systems on continuously growing domains. J Comput Phys 225:100–119

Madzvamuse A (2009) Turing instability conditions for growing domains with divergence free mesh velocity. Nonlinear Anal Theory Methods Appl 12:2250–2257

Madzvamuse A, Gaffney EA, Maini PK (2009) Stability analysis of non-autonomous reaction-diffusion systems: the effects of growing domains. J Math Biol 61:133–164

Maini PK, Painter KJ, Chau HNP (1997) Spatial pattern formation in chemical and biological systems. Faraday Trans 93:3601–3610

Murray JD (2002) Mathematical biology I and II, 3rd edn. Springer, Berlin

Plaza RG, Sánchez-Garduño F, Padilla P, Barrio RA, Maini PK (2004) The effect of growth and curvature on pattern formation. J Dynam Diff Eqs 16(4):1093–11214

Prigogine I, Lefever R (1968) Symmetry breaking instabilities in dissipative systems. II. J Chem Phys 48:1695–1700

Schnakenberg J (1979) Simple chemical reaction systems with limit cycle behaviour. J Theor Biol 81:389–400

Schmidt A, Siebert KG (2005) Design of adaptive finite element software: the finite element toolbox ALBERTA, vol 42. Lecture notes in computational science and engineering. Springer, Berlin

Turing A (1952) The chemical basis of morphogenesis. Phil Trans R Soc Lond B 237:37–72